RBMO

ARTICLE

Limitations of ploidy prediction by time-lapse morphokinetics and artificial-intelligence-based embryo selection algorithms: trisomies fly under the radar

BIOGRAPHY

Iulian C. Roman is a senior clinical embryologist and Laboratory Manager at Sims IVF Fertility Clinic in Dublin (Republic of Ireland). With a background in animal embryology and a MSc in Genetic Engineering and Reproductive Biotechnologies, his work and research are centred on the practical implementation of emerging technologies.

Iulian C. Roman[1,2,*], Graham Coull[1], Nicholas Knowlton[3,4], Tara Doherty-Eagles[1], Ogün Ozturk[1], Adriana Michielsen[1], Hannah Carty[1], Olena Yefremenkova[1], Marius Zăhan[2,5]

KEY MESSAGE

The ability to predict embryo ploidy using morphokinetic analysis or time-lapse selection algorithms is effective for detecting monosomies and complex aneuploidies. However, embryos with trisomies involving small and medium chromosomes are indistinguishable from euploid embryos.

ABSTRACT

Research question: How does the genetic constitution of embryos impact the accuracy and effectiveness of time-lapse ploidy detection?

Design: A retrospective analysis of chromosomal constitution, morphokinetic characteristics and embryo grading was conducted on 1012 embryos, originating from 386 intracytoplasmic sperm injection cycles at a single clinic. Morphokinetic checkpoints of pronuclear fading, cleavage stages and post-cleavage stages – including start of compaction; time to compacted morula; time to start of blastulation; and time to full, expanded and hatching blastocyst – were recorded for all analysed embryos. Morphokinetic profiles of 363 euploid embryos were used as reference to analyse 649 embryos with aneuploidies, according to their level of gain or loss of chromosomal material. Embryo grading was performed using commercially available time-lapse-based algorithmic embryo selection tools.

Results: Embryos with loss of genetic material and embryos with multiple aneuploidies exhibited consistent developmental delays that accumulated and became significant at the time of blastulation. In contrast, embryos with chromosomal gains displayed a morphokinetic profile almost identical to that of euploid embryos. Subset analyses suggested that aneuploidies of large chromosomes tend to have a greater impact on the morphokinetic profile. Time-lapse-based algorithmic or artificial intelligence scoring downgraded blastocysts with loss of chromosomal material or with complex aneuploidies, but discrimination potential was not observed between embryos with gain of chromosomes and euploid embryos.

[1] Sims IVF Fertility Clinic, Dublin, Republic of Ireland
[2] Department of Life Sciences and Biotechnology, University of Agricultural Sciences and Veterinary Medicine Cluj-Napoca, Cluj-Napoca, Romania
[3] Department of Obstetrics, Gynaecology and Reproductive Sciences, University of Auckland, Auckland, New Zealand
[4] School of Mathematical and Computational Sciences, Massey University, Palmerston North, New Zealand
[5] Biotechnology Research Centre, Life Sciences Institute 'King Michael I of Romania', University of Agricultural Sciences and Veterinary Medicine of Cluj-Napoca, Cluj-Napoca, Romania

KEY WORDS

Morphokinetics
Time-lapse
PGT-A
Artificial intelligence embryo selection
Aneuploidy

*Corresponding author. E-mail address: iulian.roman@sims.ie (I.C. Roman). https://doi.org/10.1016/j.rbmo.2025.104828 1472-6483/
Declaration: The authors report no financial or commercial conflicts of interest.

Conclusions: Embryos with extra chromosomes show similar morphokinetic patterns to euploid embryos, reducing the effectiveness of non-invasive selection tools. However, embryos with monosomies or multiple aneuploidies experience significant delays in reaching blastulation, and generally score lower on time-lapse selection algorithms.

INTRODUCTION

In the pursuit of enhancing outcomes in assisted reproductive technology, two primary approaches have emerged and expanded in the last decade as key drivers of innovation: preimplantation genetic testing for aneuploidy (PGT-A) and time-lapse embryo culture. Aneuploidy in embryos, a major contributor to failed implantation and pregnancy loss (*Pirtea et al., 2021*), has prompted the development of PGT-A, a genetic screening procedure based on invasive retrieval of embryonic cells, aimed at selecting chromosomally normal (euploid) embryos in preference to those with abnormal chromosomal make-up. Extensive data demonstrate the benefits of PGT-A, especially for women of advanced maternal age (*Spinella et al., 2023*), contributing to a general reduction in the miscarriage rate across the population (*Simopoulou et al., 2021*).

Simultaneously, time-lapse-based incubation, which involves continuous monitoring of embryonic development, has transformed embryo selection by integrating precise timing of developmental morphokinetics to enhance the likelihood of selecting embryos with optimal pregnancy potential (*Fishel et al., 2017*; *Pribenszky et al., 2017*). This real-time observation allows for the detection of crucial developmental milestones, potentially reducing the need for invasive genetic testing by extrapolating indicators of chromosomal health. Algorithmic grading based on morphokinetic assessment throughout embryo development has been shown to improve post-embryo transfer outcomes in terms of clinical pregnancy (*Tartia et al., 2022*) and live birth rates (*Fishel et al., 2017*). Although discrimination potential has been identified exploring various clinical factors in relation to the morphokinetic profile of human embryos, including women's age and body mass index (*Kirkegaard et al., 2016*), incidence of polycystic ovary syndrome (PCOS) (*Schachter-Safrai et al., 2021*), type of ovarian stimulation (*Muñoz et al., 2013*), quality of ovarian stimulation treatment by means of oocyte maturation rate (*Setti et al., 2022*), quality of spermatozoa used for insemination (*Kahraman et al., 2020*), and utilization of fresh versus frozen/thawed oocytes (*De Gheselle et al., 2020*; *Montgomery et al., 2023*), the most sought after is likely the correlation between morphokinetic behaviour and embryo ploidy.

The quest to harness morphokinetic profiling as a non-invasive ploidy and viability predictor has garnered substantial attention in reproductive research. Even before the implementation of time-lapse morphokinetics, oocyte morphology (*Kahraman et al., 2000*; *Navarro et al., 2009*; *Rienzi et al., 2005*), cleavage stage embryos (*Munné, 2006*) and blastocyst morphology (*Capalbo et al., 2014*) were assessed for their relationship with aneuploidy. Initial time-lapse aneuploidy studies showed that the use of early-stage milestones, such as time to pronuclear fading (tPNF), time to reach two and five cells (*Chawla et al., 2015*), and the length of initial cell cycles (*Basile et al., 2014*), may increase the probability of selecting euploid embryos. Blastomere symmetry of four-cell embryos (*Shenoy et al., 2021*) and early cleavage dynamics (*Chavez et al., 2012*) were also shown to improve selection algorithms in relation to ploidy.

With the expansion of prolonged embryo culture to the blastocyst stage, clinical practice shifted from single blastomere biopsy to trophectoderm biopsy (*Qi et al., 2014*). Consequently, the morphokinetic ploidy approach has focused increasingly on the later stages of embryo development. Time to start of blastulation (tSB) was proposed early on as the main parameter for ploidy discrimination algorithms (*Campbell et al., 2013a*,*b*), although later studies have shown that this single parameter approach is insufficient (*Kirkegaard et al., 2014*; *Kramer et al., 2014*). Nevertheless, studies have shown that although morphokinetic differences may emerge early in the cleavage stages, more significant time delays between euploid and aneuploid embryos can be observed in the post-compaction stages (*Kirkegaard et al., 2016*; *Martín et al., 2021*). The addition of variables assessed during the compaction, morula and blastulation stages of embryo development, a poorly characterized developmental period, before the introduction of time-lapse morphokinetics was shown to have ploidy discrimination potential (*De Martin et al., 2024*; *Hori et al., 2023*; *Huang et al., 2019*; *Hur et al., 2023*; *Ivec et al., 2011*; *Mumusoglu et al., 2017a*).

Further improvements in selecting embryos for clinical pregnancy were achieved by incorporating newly developed artificial intelligence (AI) selection tools (*Berntsen et al., 2022*; *Tran et al., 2019*) which make use of the imaging created by time-lapse incubation to incorporate details that exceed morphokinetic checkpoint annotations, and information that is otherwise difficult to quantify by regular observation, in their algorithms. Despite constant emergence and improvement of these technological features, time-lapse-based ploidy detection is still at an unsatisfactory level (*Banford et al., 2023*; *Kirkegaard et al., 2014*; *Rajendran et al., 2023*), with the greatest limitation being the significant overlap in morphokinetic patterns between euploid and abnormal embryos. Even incorporation of clinical parameters into algorithm design (*Mumusoglu et al., 2017b*; *Zou et al., 2022*) has not fully resolved these issues (*Kato et al., 2023*; *Lee et al., 2019*), likely due to various confounding factors (*Barrie et al., 2021*; *Kirkegaard et al., 2016*).

To understand the nature of these limitations, contemporary research is delving deeper in the finer details of the genetic architecture of the embryo. Mosaic embryos have been shown to have an intermediary morphokinetic signature between euploid and aneuploid embryos (*Martín et al., 2021*; *Zou et al., 2024*). Both decreased morphological grading and delayed morphokinetics in embryos have been associated with increasing complexity of chromosome disorders (*Hori et al., 2023*; *Del Carmen Nogales et al., 2017*) or the presence of unbalanced chromosomal translocations (*Amir et al., 2019*), while small subsets of embryos bearing non-fatal trisomies show similar morphokinetic patterns to euploid embryos (*Hori et al., 2023*).

The aim of this study was to scrutinize the morphokinetic behaviour of euploid embryos, and compare this with the behaviour of embryos harbouring specific aneuploid compositions, with regards to

the levels of gain or loss of nuclear chromosomal material, in order to determine whether specific morphokinetic traits could serve as reliable sentinels for morphokinetic detection of embryo ploidy.

MATERIALS AND METHODS

Patients

This study was a retrospective analysis of 1012 PGT-A-tested blastocysts resulted from 386 treatment cycles of 286 couples attending a private IVF clinic (Sims IVF, Dublin, Ireland) from June 2018 to June 2023. All available cycles with at least one blastocyst biopsied successfully for aneuploidy testing were included in this study, with the exception of cycles using frozen or donor oocytes. Advanced maternal age was the main clinical indication for PGT-A [≥38 years, 48.7% (188/386)], followed by multiple miscarriages [16.8% (65/386)] and multiple implantation failures [12.4% (48/386)]. Multiple indications accounted for 22% of cycles (85/386). The average age of the female partner at the time of egg retrieval was 39.6 years. All patients consented to the use of anonymized data for research purposes. The study was approved by the Virtus Group IVF Australia Ethics Committee (Project No. 193, approval date 28 August 2023).

Oocyte retrieval, denudation and ICSI

Ovarian stimulation was performed with standard short antagonist or long agonist protocols using gonadotrophins (Gonal-F, Luveris and Pergoveris; all Merck Serono, USA). Transvaginal ultrasound-guided oocyte retrieval was performed under sedation with a combination of Hypnoval (Roche, Switzerland), morphine (Unipharm, Ireland) and Zofran (GSK, Ireland), 35–36 h following human chorionic gonadotrophin injection (10,000 IU Pregnyl, Organon, UK; or Ovitrelle, Merck Serono) or agonist trigger (Suprefact 1 mg/ml; Sanofi, France), using a single lumen aspiration needle (Wallace; Cooper Surgical, UK) connected to a vacuum pump (Rocket Medical, UK).

Oocyte–cumulus complexes were recovered from follicular aspirates using a stereomicroscope in a Class II hood with a heated stage, washed in G-MOPS (Vitrolife, Sweden) and cultured in G-IVF PLUS (Vitrolife) at 37.0°C in 6% CO_2, 5% O_2 and 89% N_2 for up to 2 h before cumulus cell denudation in HYASE-10X (Vitrolife) with a 130–133 glass pipette (Vitrolife). Metaphase II oocytes were further cultured in G-TL (Vitrolife) and injected with a single spermatozoon 40–42 h post trigger.

Fertilization and embryo culture

Fertilization assessment was performed 16–18 h after intracytoplasmic sperm injection (ICSI), and 2PN fertilized zygotes were placed individually in microwells of EmbryoSlides (Unisense; Fertilitech, Denmark) in G-TL culture media overlaid with mineral oil (OVOIL; Vitrolife). A subset of 344 embryos was incubated in a time-lapse incubator immediately after ICSI insemination. EmbryoSlides were placed into the Embryoscope+ time-lapse incubator at 37.0°C, 6% CO_2, 5% O_2 and 89% N_2 for up to 148 h of culture post insemination. All culture media dishes prepared were equilibrated at least 6 h before use.

Trophectoderm biopsy

All biopsies were performed on fresh blastocysts on day 5 or day 6 following oocyte collection. Zona breaching was performed routinely at the time of biopsy by laser ablation. On average, five to 10 cells were biopsied and subsequently transferred to sterile, DNA- and RNA-free polymerase chain reaction tubes. All samples were frozen before shipment to the testing facility (Reprometa S.r.o, Brno, Czech Republic) The minimum stage and quality criteria for selection of blastocysts for biopsy and vitrification was the equivalent of 3BB according to the Gardner and Schoolcraft grading system (*Gardner and Schoolcraft, 1999*).

All embryos were biopsied in individual dishes in G-MOPS buffered medium (Vitrolife), using biopsy micropipettes with an inner diameter of 25–30 μm, on inverted microscopes equipped with Integra 3 Micromanipulator and Saturn 5 Active laser (Research Instruments, Cooper Surgical, UK).

Pre-implantation genetic screening

Individual biopsy samples were amplified using multiple displacement amplification according to the manufacturer's manual (REPLI-g single cell kit; Qiagen, Germany). Amplification success was checked on 1% agarose/0.5 x tris-borate-ethylenediaminetetraacetic acid for the presence of a DNA smear typically greater than 10 kb. Preimplantation genetic diagnosis of chromosome abnormalities was performed using massively parallel sequencing (next-generation sequencing) on a DOplify whole-genome amplification platform.

Embryo categorization

Based on PGT-A results, blastocysts were classified into five groups: euploid (no abnormal genetic findings), monosomic (bearing one or two whole chromosome monosomies or segmental losses in uniform or mosaic state), trisomic (bearing one or two whole chromosome trisomies or segmental gains in uniform or mosaic state), mixed (bearing one whole chromosome monosomy or segmental loss and one whole chromosome trisomy or segmental gain, in uniform or mosaic state) and complex (bearing three or more abnormal genetic findings).

To explore how aneuploidies of varying chromosome sizes influence morphokinetic patterns, trisomic and monosomic embryos bearing a single aneuploidy were further divided into subgroups based on the chromosome size (large, medium or small).

A validation and concordance study of the PGT-A platform, as published previously (*Navratil et al., 2020*), demonstrated a 98.3% detection rate for segmental aneuploidies within the range of seven to 31 Mb, providing robust evidence of the platform's accuracy in identifying segmental gains and losses.

Evaluation of embryo development and time-lapse-based embryo grading

All morphokinetic annotations and blastocyst grading according to Gardner and Schoolcraft's system (*Gardner and Schoolcraft, 1999*) were performed by a single experienced embryologist blinded to the PGT-A outcomes of the tested embryos. Time-lapse images were collected every 10 min throughout embryo culture to the time of embryo biopsy. Insemination time was recorded as the time of moving the denuded oocyte into the ICSI dish + 5 min. The exact timing of variables was annotated as described elsewhere (*Ciray et al., 2014*): tPNf; divisions to two, three, four, five, six, seven, eight and nine cells (t2, t3, t4, t5, t6, t7, t8 and t9); start of compaction (tSC); compacted morula (tM); start of blastulation (tSB); blastocyst (tB); expanded blastocyst (tEB); and time of blastocyst hatching

(tHB). Timings were expressed in hours post insemination or as hours post pronuclear fading. All PGT-A-tested embryos were subjected to grading using one time-lapse-based algorithmic model (KIDScore v.3.2; Vitrolife) and three different, commercially available, time-lapse-based embryo selection tools. The embryo selection tools are described as artificial-intelligence (AI)-based algorithms that were developed using time-lapse-based video sequences as input and fetal heart activity as an end point (*Ahlström et al., 2023*; *Berntsen et al., 2022*; *Duval et al., 2023*). In this study, the video scores alone were used for assessment, with no additional demographic or clinical data included in the scoring process. The decision to rely exclusively on video data aimed to provide an unbiased assessment focused purely on the morphological and kinetic features observed during embryo development, without the influence of external patient-specific factors.

Statistical analysis

In order to assess the impact of ploidy on morphokinetics, no clustering analysis with regards to embryos from same cycle or patients was required. A linear mixed-effects model was used to investigate the influence of ploidy on embryo morphokinetics. For this model, timing data were pre-processed by subtracting tPNf on an embryo-specific basis to reduce the effect of oocyte insemination timing within a culture dish, and to use a more objective internal measure to start timing.

The model was designed to analyse the fixed effects of ploidy (categorized as euploid, trisomic, monosomic, mixed and complex), morphokinetic stage (e.g. t2, tM) and their interaction. This allowed assessment of the association between ploidy types and changes in time since fertilization across different morphokinetic stages.

Random intercepts were incorporated for each embryo, accounting for the intrinsic variability in morphokinetics attributable to individual differences. Furthermore, an autoregressive [AR(1)] correlation structure was specified to model the serial correlation of measurements within each embryo across successive developmental stages, acknowledging that measurements closer in time are likely more correlated. The statistical model can be formally represented as follows:

$$\begin{aligned}\text{Time} = {} & \beta 0 + \beta 1\ (\text{ploidy}) \\ & + \beta 2\ (\text{stage}) \\ & + \beta 3\ (\text{ploidy x stage}) + \text{b0i} \\ & + \epsilon \text{ij}\end{aligned}$$

where $\beta 0$ is the overall intercept; and $\beta 1$, $\beta 2$ and $\beta 3$ represent the fixed effects coefficients for ploidy, stage and their interaction, respectively. b0i denotes the random intercept for each embryo, capturing individual variability, and ϵij is the residual error for the i-th embryo at the j-th stage, with ϵij following an AR(1) process.

Post-hoc analyses were conducted to test specific differences in development time among the ploidy groups at each developmental stage. This involved estimating the estimated marginal means for each ploidy group compared with the euploid reference group, with *P*-values adjusted for multiple comparisons using Dunnett's correction. All statistical analyses were executed using R Version 4.3.3 (R Foundation, Austria) or SPSS Version 29.0.1 (IBM, USA) with an alpha level of 0.05 denoting statistical significance. Comparison of age distribution between embryo groups was assessed using one-way analysis of variance adjusted by Tukey's honestly significant difference post-hoc test. A conservative Kruskal–Wallis test was used for the analysis of embryo subgroups and scoring of embryo selection tools due to smaller sample sizes. Nominal *P*-values were adjusted for multiplicity using Bonferroni's method.

RESULTS

PGT-A testing revealed euploidy in 363 (35.9%) blastocysts, presence of excess chromosomal material (trisomic) in 174 (17.2%) blastocysts, loss of chromosomal material (monosomic) in 211 (20.8%) blastocysts, presence of one trisomy or segmental gain and one monosomy or segmental loss (mixed) in 60 (5.9%) blastocysts, and incidence of three or more chromosomal aneuploidies (complex) in 204 (20.2%) blastocysts. Live birth following single embryo transfer was documented for 111 embryos (106 euploid embryos, four embryos with a single mosaic monosomy, and one embryo with a single mosaic trisomy).

The age of the female partner at the time of oocyte retrieval was recorded for each embryo. The mean age differed significantly across the embryo groups, with increases for all aneuploidy subgroups ($P < 0.001$) in comparison with the euploid group (**TABLE 1**). The distribution for each embryo group by age is displayed in **FIGURE 1**. The distribution of aneuploidies for each chromosome is indicated in **FIGURE 2**. The analysis of aneuploidy in this dataset reveals distinct patterns across different chromosomes. Whole chromosome abnormalities (trisomies and monosomies) affected all chromosomes with the exception of chromosome Y, with the highest prevalence in chromosomes 15, 16, 21 and 22. In terms of segmental aneuploidies, chromosome 9 had the highest occurrence of uniform segmental gains, while chromosome 4 had the highest incidence of uniform segmental losses. Mosaic aneuploidies also showed substantial variation, with chromosome 22 exhibiting the highest frequency of mosaic trisomy and monosomy, while mosaic segmental aneuploidies were more common in larger chromosomes and chromosome 13. Sex chromosome aneuploidies were present but less frequent, with chromosome X anomalies being present in all types, and a single case of segmental gain was detected for chromosome Y.

From the 174 embryos included in the trisomic group, 137 (78.7%) were found to carry uniform aneuploidies alone, 34 (19.5%) were found to carry mosaic aneuploidies alone, and three (1.7%) were found to carry both uniform and mosaic trisomies.

From the 211 embryos included in the monosomic group, 160 (75.8%) were found to carry uniform aneuploidies alone, 40 (19.0%) were found to carry mosaic aneuploidies alone, and 11 (5.2%) were found to carry both uniform and mosaic monosomies.

From the 60 embryos included in the mixed group, 38 (63.3%) were found to carry uniform aneuploidies alone, one (1.6%) was found to carry mosaic aneuploidies alone, and 21 (35%) were found to carry one uniform aneuploidy and one mosaic aneuploidy.

TABLE 1 COMPARISON OF AGE AT OOCYTE RETRIEVAL BETWEEN PLOIDY GROUPS

Embryo group	*n*	Mean age[a]	SD	SE	95% CI for mean		Min.	Max.
					Lower bound	Upper bound		
Euploid	363	37.39[b]	3.401	0.179	37.04	37.74	27.5	45.6
Trisomic	174	39.28[c]	3.409	0.258	38.76	39.79	27.5	46.2
Monosomic	211	39.12[c]	3.027	0.208	38.71	39.53	29.1	45.7
Mixed	60	40.32[c,d]	3.316	0.428	39.46	41.17	30.5	46.2
Complex	204	40.50[d]	3.253	0.228	40.05	40.95	30.4	45.7
Total	1012	38.87	3.505	0.110	38.66	39.09	27.5	46.2

[a] One-way analysis of variance comparison followed by Tukey honestly significant difference post-hoc test. Based on observed means.
Different superscript letters denote significant differences between groups at the 0.05 level. All significant differences listed have $P < 0.001$ with the exception of trisomic versus complex where $P = 0.003$.

From the 204 embryos included in the complex group, 72 (35.3%) were found to carry uniform multiple aneuploidies alone, 36 (17.6%) were found to carry mosaic multiple aneuploidies alone, 90 (44.1%) were found to carry different combinations of uniform and mosaic aneuploidies, and six (2.9%) were triploid embryos. The detailed distribution of aneuploidies for each embryo group is indicated in FIGURE 3.

Morphokinetic analysis

The baseline descriptives of morphokinetic variables recorded for the 1012 embryos analysed are shown in Supplementary Table 1. At the time of trophectoderm biopsy, 71 (7%) embryos were at the full blastocyst stage, 400 (39.5%) were in the expansion phase, and 541 (53.5%) had started hatching. Fifteen morphokinetic variables were analysed among the embryos of the different ploidy groups.

By applying the linear mixed-effects model, a developmental timing difference was observed in the monosomic group from tB ($P = 0.002$) through tEB ($P < 0.001$) and tHB ($P < 0.001$) in comparison with the euploid group. A similar trend was observed in the complex group where both tEB ($P = 0.0182$) and tHB ($P = 0.0168$) were delayed in comparison with the euploid group (Supplementary Table 2). As a result, all embryo groups had similar developmental trajectories during the cleavage stages, but starting from tSC, both monosomic and complex embryo groups started to accumulate delays (FIGURE 4), which resulted in significant differences around the blastulation stages (FIGURE 5). The mixed group seemed to have a shorter transition from t9 to tM, but required a longer period until they started forming the blastocoelic cavity, which resulted in delayed blastulation events; this finding did not reach significance due to the small size of this group. The trisomic group was shown to be constantly faster than all other groups during the cleavage and compaction stages, although the gap between the trisomic and euploid groups narrowed from tM to tHB to very similar checkpoint timings. No significant differences were observed between the trisomic and euploid groups for any of the variables assessed.

Embryo grading using time-lapse-based AI selection tools further accentuated the differences between the morphokinetic profiles of the analysed ploidy groups, demonstrating a greater discriminative potential than morphokinetic analysis alone. The euploid and trisomic embryos consistently achieved higher scores across all time-lapse-based selection tools in

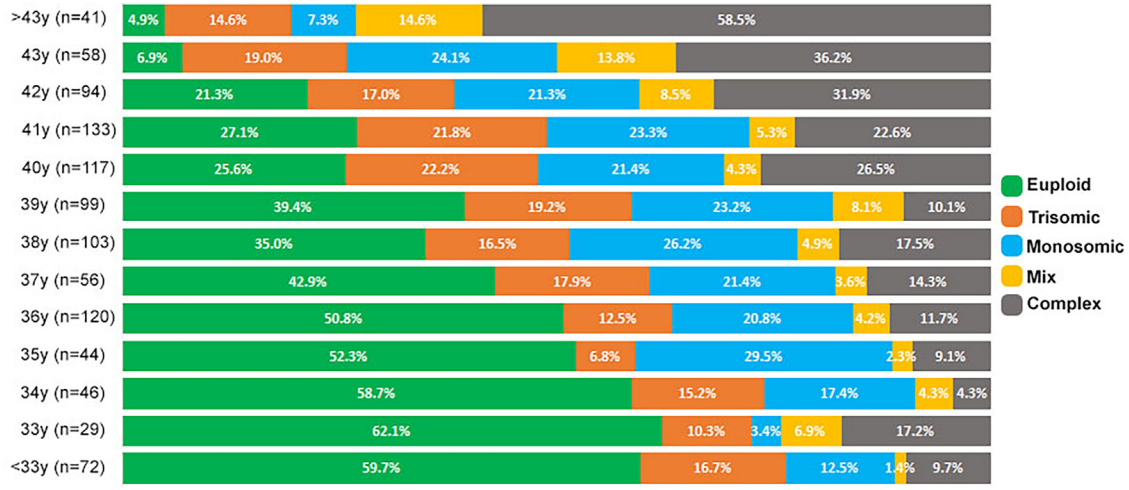

FIGURE 1 Frequencies of different ploidies according to maternal age at oocyte retrieval. Green bars, euploid; orange bars, trisomic; blue bars, monosomic; yellow bars, mixed, dark grey bars, complex.

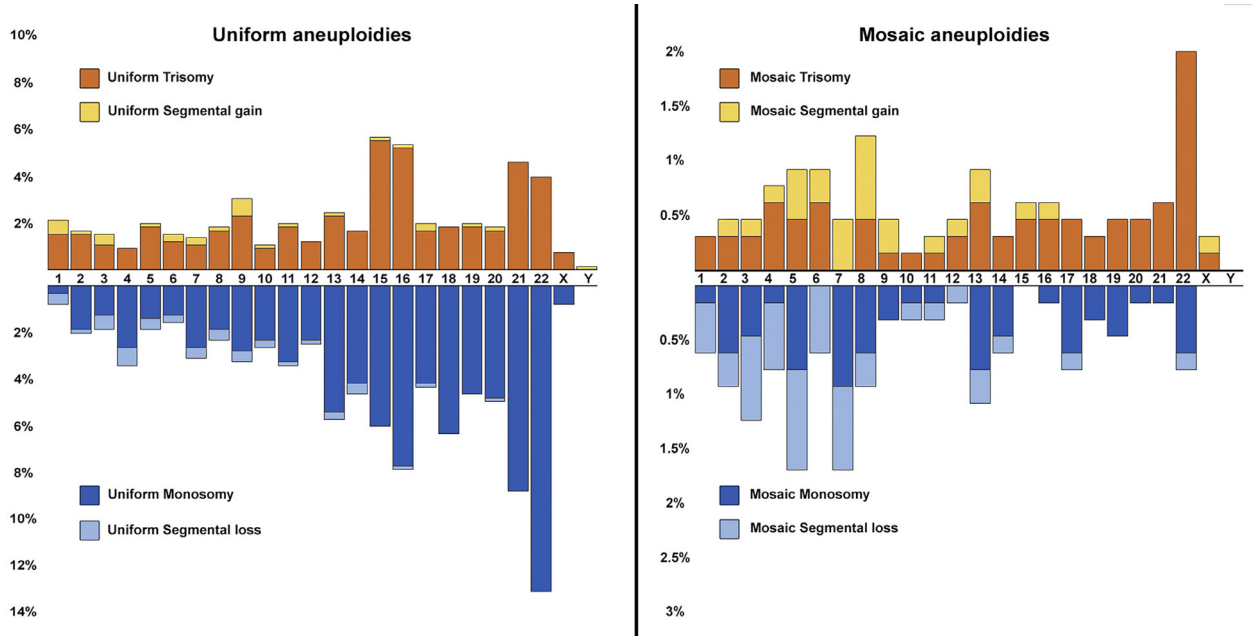

FIGURE 2 Chromosome aneuploidy type and frequencies detected in 1012 biopsied embryos. Right bar chart depicts the frequency of aneuploidies detected in all biopsied cells (uniform). Left bar chart depicts the frequency of aneuploidies detected in a mosaic state. Bars pointing upwards represent gain of chromosomal material as whole chromosome trisomy (orange bars) or as chromosomal segmental gains (yellow bars). Bars facing downwards represent loss of chromosomal material by means of whole chromosome monosomy (dark blue bars) or as chromosomal segmental losses (light blue bars).

comparison with the monosomic, mixed and complex embryos (FIGURE 6), with significant differences found between these groups (TABLE 2).

To investigate whether the size of chromosomes involved in aneuploidies affects embryo morphokinetic profiles differently, 167 monosomic embryos and 139 trisomic embryos with a single detected aneuploidy were divided into subgroups based on chromosome size: large (chromosomes 1–8 and X), medium (chromosomes 9–16), and small (chromosomes 17–22 and Y). A pairwise non-parametric comparison between these subgroups and a reference set of 111 embryos that led to live births revealed significant delays in at least one morphokinetic variable associated with blastulation stage across all monosomic subgroups. Specifically, significant differences were observed between live birth embryos and those with small chromosome monosomies at tSB ($P = 0.046$), tB ($P = 0.03$) and tEB ($P = 0.032$). Additionally, embryos with medium chromosome monosomies had significant delays ($P \leq 0.046$) at tB and tHB, while delays for those with large chromosome monosomies reached significance at tHB ($P = 0.037$). (Supplementary Table 3). The morphokinetic trajectory indicated a shift from the live birth embryo pattern for all monosomic subgroups starting from tSB (FIGURE 7A). No significant differences were identified between live birth embryos and the trisomic subgroups (Supplementary Table 4), although trisomies of large chromosomes appear to progress more slowly in the post-cleavage stages (FIGURE 7B).

Time-lapse-based embryo scoring for these subsets of embryos indicated downgrading for all monosomic embryos and those with trisomies of large chromosomes (FIGURE 8). Significantly lower scores were detected for all monosomic subgroups in comparison with live birth embryos with the use of two time-lapse-based selection tools and the KIDScore (all $P \leq 0.05$), while scoring of one of the time-lapse-based selection tools did not generate significant differences between live birth embryos and embryos with large chromosome monosomies. Further significant differences were observed between monosomic and trisomic subgroups (all $P < 0.026$) (TABLE 3), while no significant differences were detected between embryos with large chromosome trisomies and any of the monosomic subgroups (Supplementary Table 5).

DISCUSSION

A common approach in studies examining the relationship between morphokinetics and embryo ploidy has been to classify embryos as either normal or abnormal (*Patel et al., 2016*), or to compare euploid embryos with a broad category of aneuploid embryos (*Banford et al., 2023*; *Minasi et al., 2016*). By segregating the embryos with abnormal chromosomal findings according to their level of chromosomal material gain or loss, the present study has shown that different types of aneuploidies underline variable morphokinetic profiles.

These results indicate that the presence of monosomies in the chromosomal complement of embryos affects their morphokinetic profile significantly, introducing delays that accumulate and become pronounced by the time of blastulation. This is consistent with

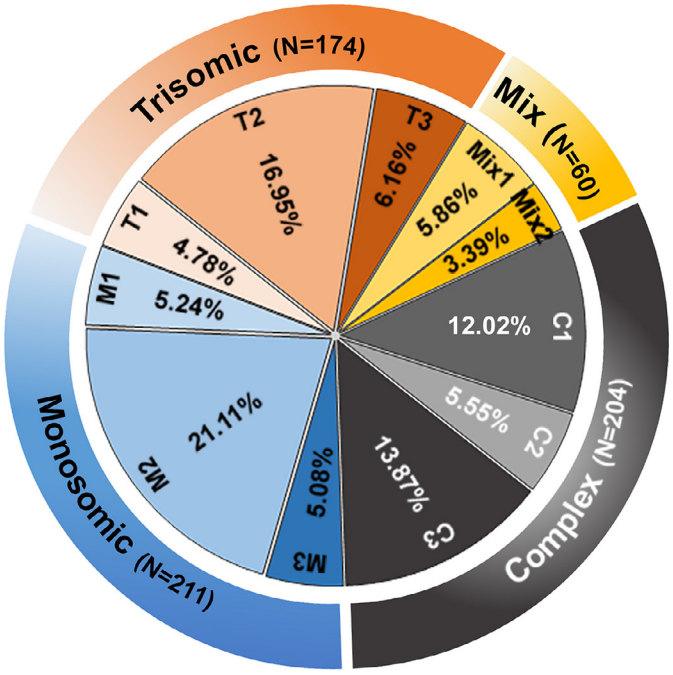

FIGURE 3 Detailed representation of the frequency and distribution of various aneuploidy categories in embryos analysed through preimplantation genetic testing for aneuploidy. T1, embryos with a single mosaic trisomy or segmental gain; T2, embryos with a single uniform trisomy or segmental gain; T3, embryos with two trisomies or segmental gains, in either uniform and/or mosaic states; M1, embryos with a single mosaic monosomy or segmental loss; M2, embryos with a single uniform monosomy or segmental loss; M3, embryos with two monosomies or segmental losses, in either uniform and/or mosaic states; Mix1, embryos presenting one monosomy/segmental loss and one trisomy/segmental gain, both in a uniform state; Mix2, embryos with one monosomy/segmental loss and one trisomy/segmental gain, occurring in both uniform and mosaic states; C1, embryos affected by three or more uniform aneuploidies; C2, embryos affected by three or more mosaic aneuploidies; C3, embryos exhibiting three or more aneuploidies, with a combination of uniform and mosaic states.

previous findings which show that monosomies have a significant effect on embryo arrest prior to blastulation (*De Munck et al., 2021*), with an overall slower development rate (*Alfarawati et al., 2011*). It is believed that monosomic embryos have a lower implantation potential, taking into account that autosomal monosomies are rarely detected in first-trimester miscarriages, while the only monosomic aneuploidies compatible with full term pregnancy are those of the sex chromosomes (*Munné, 2006*). A recent study using one AI model trained on single day 5 static images found that embryos containing a single monosomy were almost eight-fold more likely to be found in the lowest scoring category (*Diakiw et al., 2022a*), highlighting the impact of monosomies on blastocyst morphology and slow pace to reach this stage. In the present dataset, the trajectory of monosomic and mixed groups, which contain embryos with at least one monosomy, started to separate from the euploid and trisomic groups within the fourth round of blastomere cleavage, and became more pronounced following morulation.

It was not possible to distinguish a particular pattern by segregating the embryos bearing a single monosomy according to the size of the chromosome implicated in the aneuploidy, most likely due to the small size of the samples. In comparison with live birth embryos, monosomies of all chromosome sizes had similar delayed morphokinetics, with statistical significance being reached towards the later stages of blastulation. This finding was also depicted by the time-lapse-based selection tools, with all of them downgrading monosomies of all chromosome sizes to a significant level in comparison with live birth embryos and certain subgroups of trisomic embryos.

Embryos with complex aneuploidies are often considered to be the most problematic among aneuploid embryos. They have been reported to have the highest rates of developmental arrest (*De Munck et al., 2021*), and are frequently found within poor-quality blastocysts (*Quinn et al., 2022*). Typically, these embryos exhibit slow development

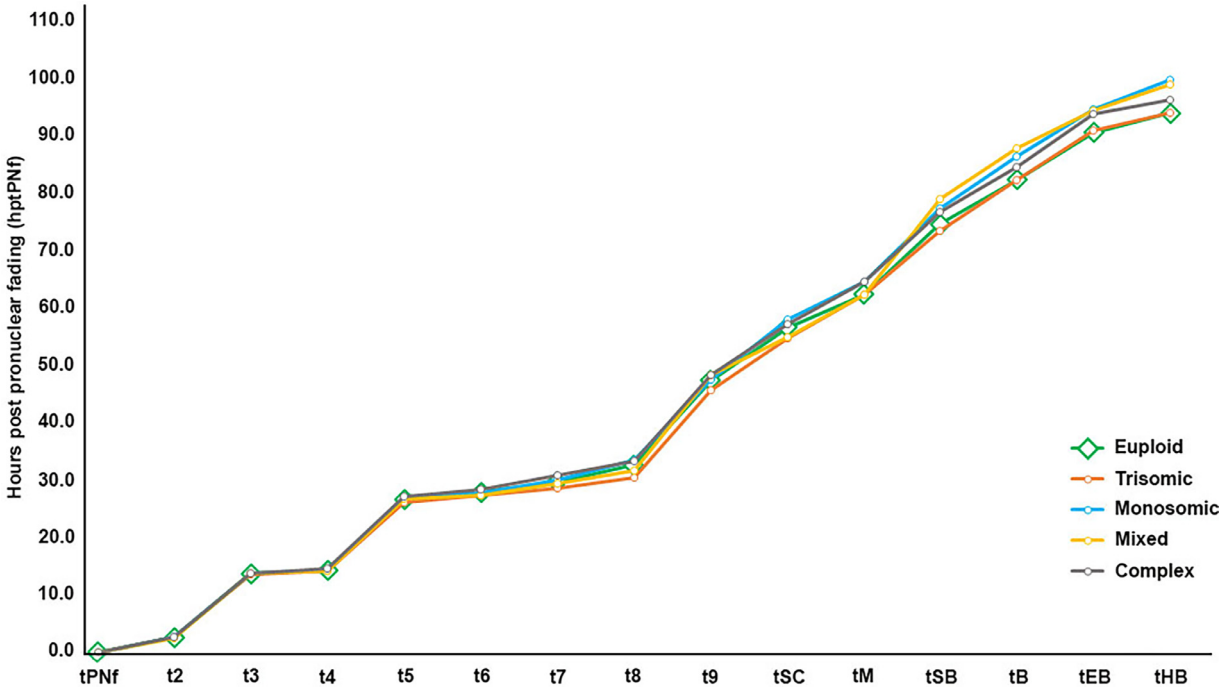

FIGURE 4 Morphokinetic trajectory of embryos. Morphokinetic checkpoints represented by green diamonds (euploid), orange circles (trisomic), blue circles (monosomic), yellow circles (mixed) and dark grey circles (complex) depict the median value for each embryo group. tPNf, both pronuclei faded/syngamy; t2, t3, t4, t5, t6, t6, t7, t8 and t9, two-, three-, four-, five-, six-, seven-, eight- and nine-cell stage, respectively; tSC, start of compaction; tM, compacted morula; tSB, start of blastulation; tB, full blastocyst stage; tEB, expanded blastocyst; tHB, blastocyst hatching.

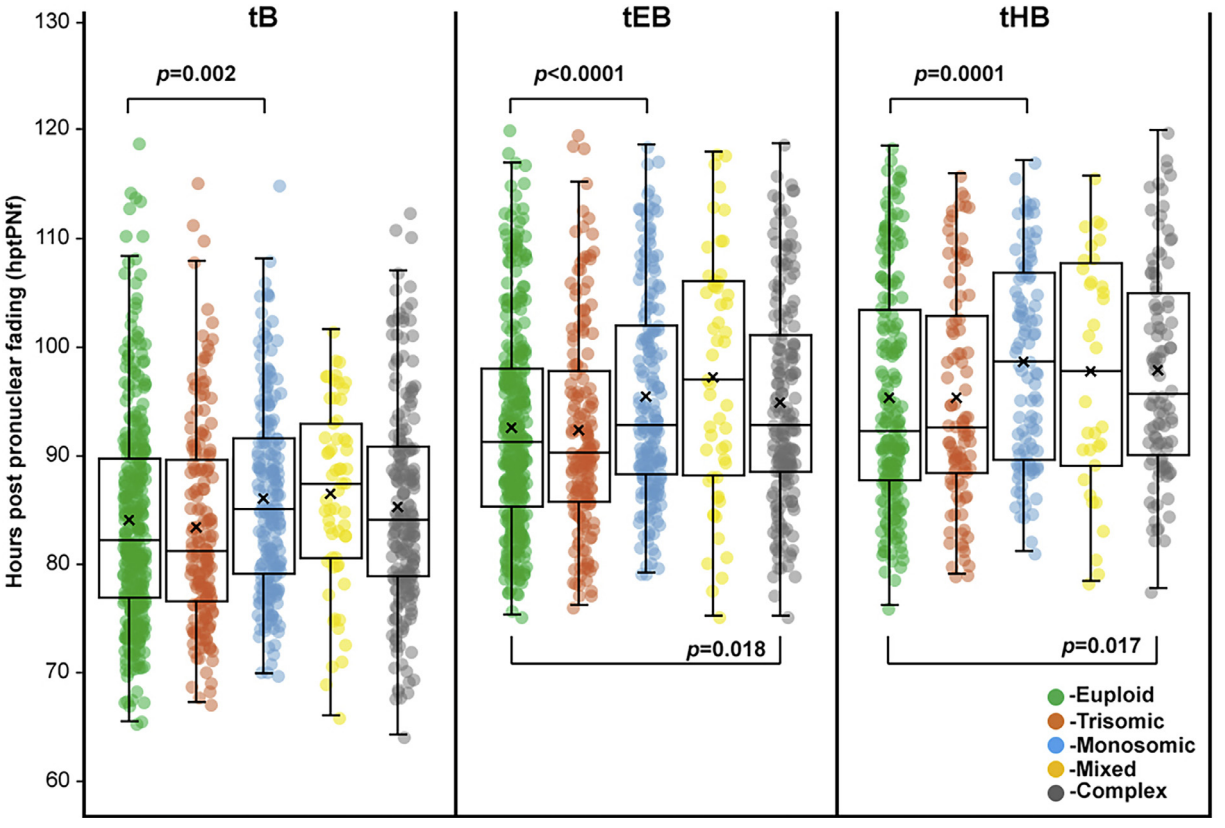

FIGURE 5 Distribution of morphokinetic timing according to embryo ploidy. Box plots show the median and quartile ranges. Dots represent individual morphokinetic timing of each embryo sample. tB, full blastocyst stage; tEB, expanded blastocyst; tHB, blastocyst hatching. Green dots, euploid; orange dots, trisomic; blue dots, monosomic; yellow dots, mixed; dark grey dots, complex. Figures show significant *P*-values for comparisons using linear mixed-effects model versus euploid group; for all other *P*-values versus euploid group, see Supplementary Table 2.

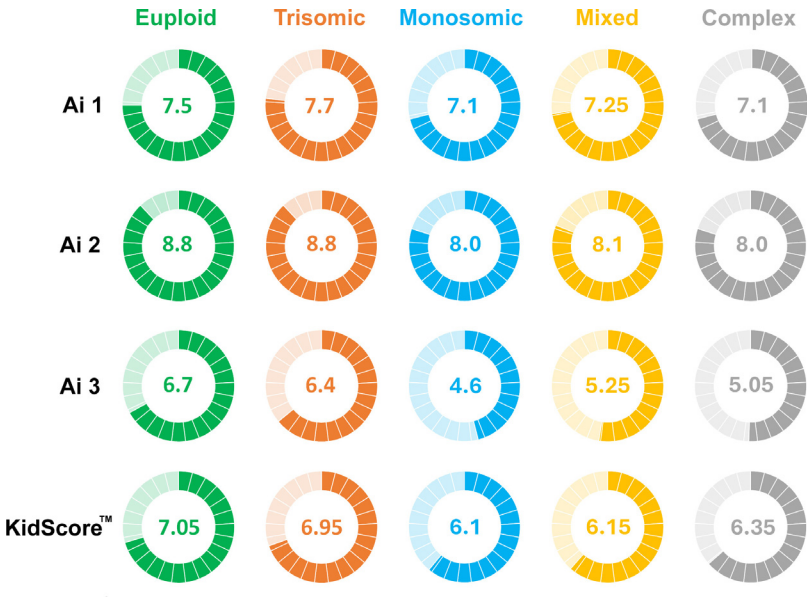

FIGURE 6 Embryo scoring according to embryo ploidy. Centre number indicates the median score for each ploidy group for each artificial-intelligence time-lapse-based and KIDScore algorithm. Green, euploid; orange, trisomic; blue, monosomic; yellow, mixed; grey, complex.

(*Alfarawati et al., 2011*) and lower expansion rates post blastulation (*Hori et al., 2023*). Additionally, complex aneuploidy in a mosaic state has been linked to reduced chances of implantation and live birth following the transfer of mosaic embryos (*Viotti et al., 2021*). The incidence of complex aneuploidy is associated with increased maternal age (*Qi et al., 2014*) and the use of testicular-retrieved spermatozoa (*Kahraman et al., 2020*). The present findings confirm the significant trend of increasing incidence of complex chromosomal rearrangements with advancing maternal age. This observation aligns with the well-documented decline in oocyte quality associated with advanced maternal age. Specifically, the present data reveal that the proportion of embryos classified within the complex group increased consistently with age. This occurred at the expense of the euploid group, while the incidence of trisomic and monosomic embryos remained relatively constant for all age groups analysed in this dataset (FIGURE 1). It has been suggested that complex aneuploid embryos are likely to arise from the fusion of chromatin-containing embryo fragments with blastomeres during the cleavage stages (*Chavez et al., 2012*). Although one might expect this group of embryos to be easily identified through morphokinetic analysis due to the substantial impact of multiple aneuploidies on cell cycles, several AI-based ploidy prediction models have struggled to distinguish between embryos with single or multiple aneuploidies (*Diakiw et al., 2022b*; *Rajendran et al., 2023*). In the present dataset, complex embryos exhibited an intermediary morphokinetic pattern between monosomic and euploid embryos, with significant differences only starting to emerge from tB. Previous studies have shown that mosaic embryos exhibit an intermediate morphokinetic profile compared with euploid and aneuploid embryos (*De Martin et al., 2024*; *Zou et al., 2024*). This intermediate profile may be linked with the higher occurrence of mosaic aneuploidies in complex embryos, with 62% carrying at least one mosaic aneuploidy, compared with trisomic and monosomic embryos, where less than 25% exhibit such abnormalities.

A study by *Del Carmen Nogales et al. (2017)*, which used the time of insemination as the starting point for analysis, demonstrated that early morphokinetic variables have strong potential for discriminating against embryos with complex chromosomal abnormalities. Using tPNf as the starting point offers the advantage of eliminating the imprecision associated with using a standardized time of insemination, as most widely available time-lapse morphokinetics software cannot record individual insemination times for each oocyte. However, this approach can lead to the uniformity of morphokinetic patterns, particularly for early events (*Liu et al., 2015*).

A pairwise comparison analysis conducted on a subset of 344 embryos, for which the timing of the second polar body extrusion was available, revealed several morphokinetic delays in the early stages for

TABLE 2 COMPARISON OF EMBRYO SCORING BY ARTIFICIAL INTELLIGENCE TOOLS

Embryo scoring tool	Group 1	Median	IQR	versus	Group 2	Median	IQR	*P*-value[a]	Adjusted *P*-value[b]
AI 1	Euploid	7.50	1.10	versus	Trisomic	7.70	0.95	0.962	1.000
					Complex	7.10	1.43	<0.0001	<0.0001
					Mixed	7.25	1.18	0.002	0.025
					Monosomic	7.10	1.80	<0.0001	0.000
	Trisomic	7.70	0.95	versus	Complex	7.10	1.43	<0.0001	<0.0001
					Mixed	7.25	1.18	0.005	0.053
					Monosomic	7.10	1.80	<0.0001	0.000
AI 2	Euploid	8.80	1.60	versus	Trisomic	8.80	1.85	0.520	1.000
					Complex	8.00	2.00	<0.0001	<0.0001
					Mixed	8.10	2.03	0.001	0.010
					Monosomic	8.00	2.30	<0.0001	<0.0001
	Trisomic	8.80	1.85	versus	Complex	8.00	2.00	<0.0001	0.003
					Mixed	8.10	2.03	0.008	0.078
					Monosomic	8.00	2.30	0.001	0.012
AI 3	Euploid	6.70	3.50	versus	Trisomic	6.40	3.58	0.789	1.000
					Complex	5.05	3.80	<0.0001	<0.0001
					Mixed	5.25	4.30	<0.0001	0.007
					Monosomic	4.60	3.50	<0.0001	<0.0001
	Trisomic	6.40	3.58	versus	Complex	5.05	3.80	<0.0001	<0.0001
					Mixed	5.25	4.30	0.003	0.028
					Monosomic	4.60	3.50	<0.0001	<0.0001
KIDScore	Euploid	7.05	2.90	versus	Trisomic	6.95	2.60	0.530	1.000
					Complex	6.35	2.33	<0.0001	<0.0001
					Mixed	6.15	2.45	<0.0001	0.002
					Monosomic	6.10	2.00	<0.0001	<0.0001
	Trisomic	6.95	2.60	versus	Complex	6.35	2.33	<0.0001	0.004
					Mixed	6.15	2.45	0.002	0.023
					Monosomic	6.10	2.00	0.001	0.010

Each row tests the null hypothesis that the Group 1 and Group 2 distributions are the same.

p value*- nominal significance from a 2-sided Kruskal Wallis test.

[a] Nominal significance from a two-sided Kruskal-Wallis test.

[b] Adjusted for multiplicity using Bonferroni's correction.

AI, artificial intelligence.

monosomic and complex embryos in comparison with euploid embryos, specifically for tPNf, t2, t3, t4, t5, t6 and t7, which were not apparent when tPNf was excluded from the analysis (data not shown). This finding suggests that time of second polar body extrusion might be a more reliable starting point of analysis for ICSI-inseminated oocytes.

Despite the possible confounding effects generated by the choice of analysis starting point, all time-lapse-based selection tools consistently downgraded the complex, mixed and monosomic embryos, generating significant lower scores in comparison with the euploid and trisomic embryos, emphasizing greater discrimination potential of these tools against morphokinetic analysis alone.

The main finding of this study is that embryos affected by a limited number of trisomies have a morphokinetic profile that largely overlaps that of euploid embryos. None of the morphokinetic variables analysed between trisomic and euploid embryos showed any tendency for discrimination, regardless of the choice of starting point for analysis (data not shown). These findings confirm previous research based on static imaging, indicating that fast growing aneuploid embryos were more often affected by trisomies than monosomies (*Alfarawati et al., 2011*). It was also highlighted that trisomic embryos develop into top-quality day 3 embryos to a higher extent (*Tschare et al., 2023*), while morphokinetic similarities between trisomic and euploid embryos were documented for the early cleavage stages (*Del Carmen Nogales et al, 2017*).

None of the time-lapse-based selection tools or the KIDScore algorithm were able to distinguish significantly between trisomic and euploid embryos. Both the euploid and trisomic groups constantly scored higher than the monosomic, mixed and complex groups across all selection tools. A recent study based on an AI

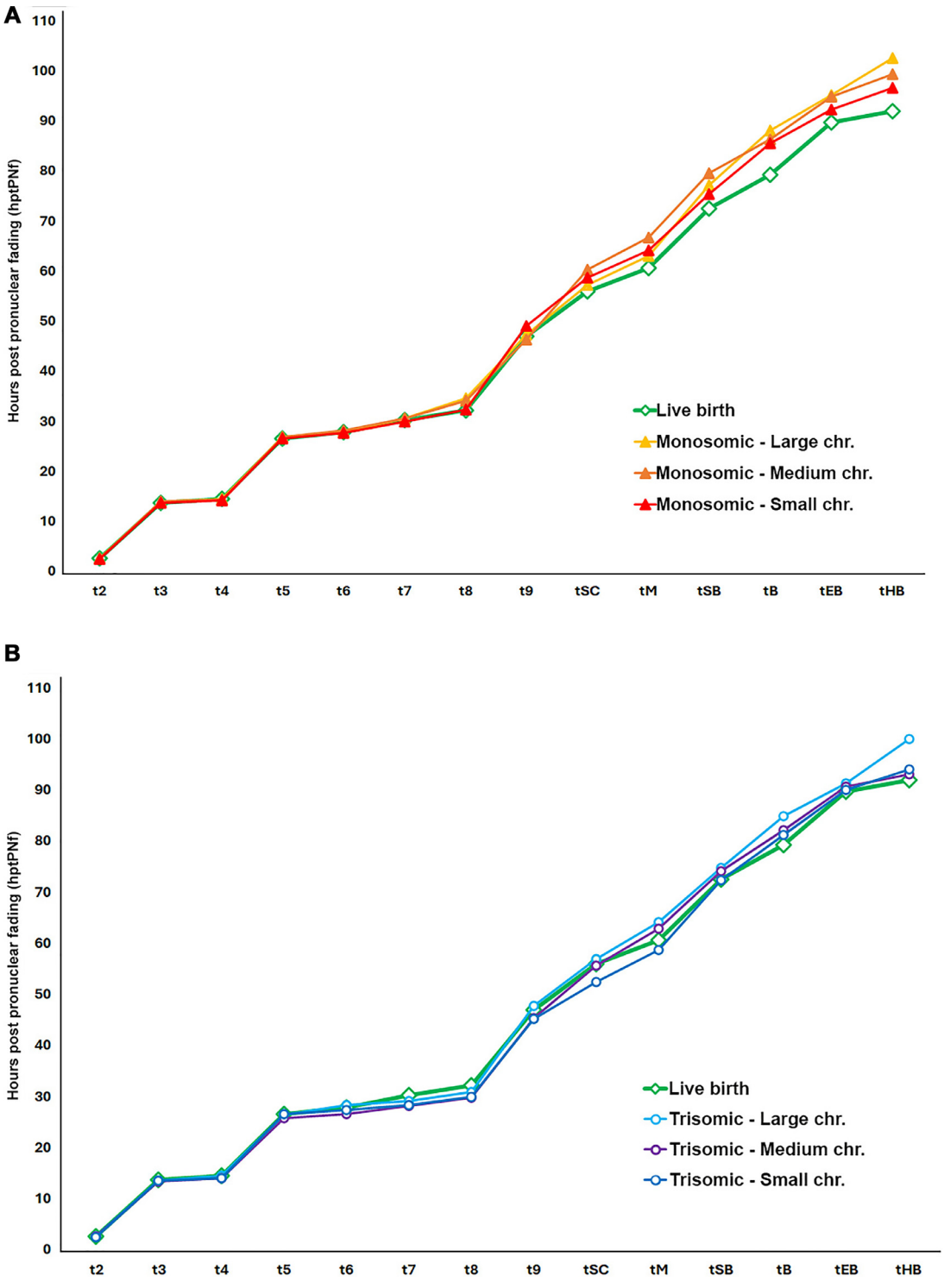

FIGURE 7 Morphokinetic trajectory comparison between live birth embryos and subsets of monosomic (A) and trisomic (B) embryos according to chromosome size. Green diamonds (live birth), red triangles (monosomic small chromosomes), orange triangles (monosomic medium chromosomes), yellow triangles (monosomic large chromosomes), dark blue circles (trisomic small chromosomes), purple circles (trisomic medium chromosomes) and light blue circles (trisomic large chromosomes) represent the median value of morphokinetic variables. t2, t3, t4, t5, t6, t6, t7, t8 and t9, two-, three-, four-, five-, six-, seven-, eight- and nine-cell stage, respectively; tSC, start of compaction; tM, compacted morula; tSB, start of blastulation; tB, full blastocyst stage; tEB, expanded blastocyst; tHB, blastocyst hatching; large chr., chromosomes 1–8 and X; medium chr., chromosomes 9–16; small chr., chromosomes 17–22 and Y.

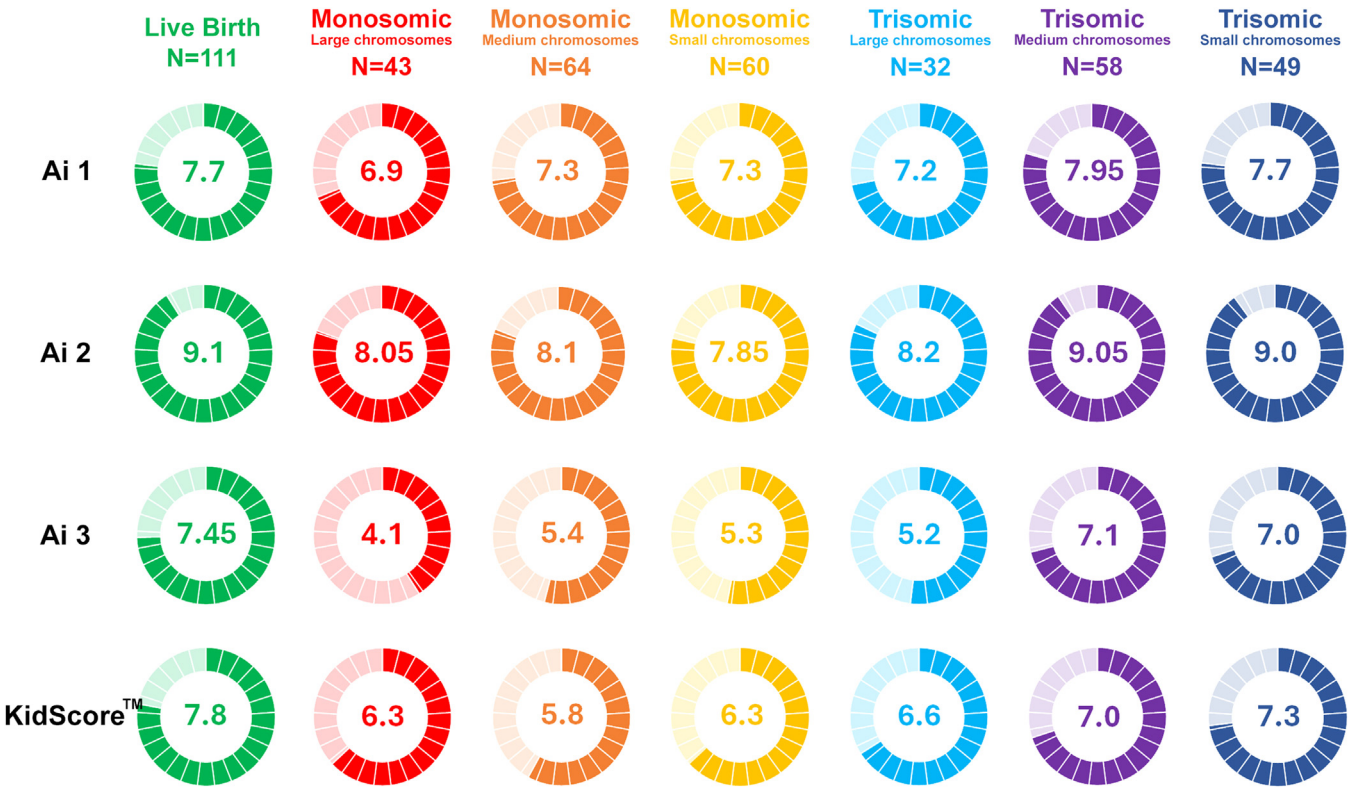

FIGURE 8 Embryo scoring comparison between live birth embryos and embryos with single aneuploidy according to chromosome size. Centre numbers indicate the median scoring value for each artificial-intelligence time-lapse-based and KIDScore algorithm.

algorithm trained using static images of blastocysts on day 5 (*Diakiw et al., 2022a*) indicated a more pronounced difference in grading between embryos with a single trisomy and euploid embryos, although in a follow-up study by the same group (*Diakiw et al., 2022b*) with an increased number of cases, these differences fell below the level of significance, more consistent with the present findings.

Within the trisomic group, some interesting findings were noted considering the size of the chromosome indicted in the aneuploidy. Embryos bearing small and medium chromosome trisomies were shown to have a faster-developing trajectory from the second round of blastomere cleavages until early blastulation, while tB and the following blastulation events fell behind in comparison with a subset of embryos that resulted in live birth following embryo transfer; however, these differences did not reach significance. This finding may suggest that the presence of these trisomies contributes to shortening of the cell cycle throughout the cleavage stages, and may explain the intermediary profile displayed by mixed embryos.

It has been shown previously that within the trisomic embryos, those with non-fatal aneuploidies (trisomies of chromosomes 13, 18 and 21) have a blastocyst expansion profile similar to euploid embryos (*Hori et al., 2023*). The present results highlight the increased implantation potential of these embryos, in concordance with previous research showing that embryos containing small and medium chromosome trisomies represent the majority of single aneuploidies identified in first-trimester miscarriages in both natural conception and IVF cycles (*Pylyp et al., 2018*).

Trisomies involving large chromosomes exhibited a slower morphokinetic profile and were consistently downgraded by all time-lapse-based selection tools used in this study. One of the AI selection tools employed downgraded embryos with large chromosome trisomies significantly more often compared with live birth embryos. One possible explanation for this is that large chromosomes are impacted to a greater extent by segmental aneuploidies. In this dataset, the aneuploidies were segmental in 36.4% (12/33) of embryos with large chromosome trisomies and 38.6% (17/44) of embryos with large chromosome monosomies, while the incidence of segmental aneuploidies in the small chromosomes was below 2%. It has been shown previously that segmental aneuploidies predominantly affect chromosomes of paternal origin (*Kubicek et al., 2019*), and that high DNA fragmentation of sperm chromatin is associated with increased incidence of segmental chromosomal aneuploidy (*Gao et al., 2023*). The information on embryos with segmental aneuploidies is limited and somewhat contradictory. While segmental mosaicism is often prioritized when considering implantation and live birth rates in mosaic embryo transfers (Viotti et al., 2020), another study highlighted a significant reduction in live birth rates for these embryos (*Zore et al., 2019*). Segmental duplications have been linked with increased risk of embryo development arrest (*De Munck et al., 2021*). Recent research showed that, like uniform chromosome aneuploidies, segmental aneuploid embryos reaching the blastocyst stage expanded more slowly than euploid embryos (*Hori et al., 2023*), although static AI scoring algorithms downgraded segmental

TABLE 3 COMPARISON OF EMBRYO SCORING BETWEEN LIVE BIRTH EMBRYOS AND EMBRYOS WITH SINGLE ANEUPLOIDY GROUPED BY THE SIZE OF THE CHROMOSOME: LIST OF SIGNIFICANT PAIR COMPARISONS

Embryo scoring tool	Group 1	Median	IQR	versus	Group 2	Median	IQR	*P*-value[a]	Adjusted *P*-value[b]
AI 1	Live birth	7.70	0.80	versus	Monosomic small chr.	7.30	1.18	<0.0001	0.001
					Monosomic medium chr.	7.30	1.50	<0.0001	0.002
	Trisomic small chr.	7.70	1.00	versus	Monosomic small chr.	7.30	1.18	0.001	0.011
					Monosomic medium chr.	7.30	1.50	0.001	0.023
	Trisomic medium chr.	7.95	0.70	versus	Monosomic small chr.	7.30	1.18	<0.0001	0.008
					Monosomic medium chr.	7.30	1.50	0.001	0.018
AI 2	Live birth	9.10	1.03	versus	Monosomic small chr.	7.85	2.15	<0.0001	<0.0001
					Monosomic medium chr.	8.10	1.60	0.001	0.020
					Monosomic large chr.	8.05	2.55	<0.0001	0.001
					Trisomic large chr.	8.20	1.60	0.002	0.049
AI 3	Trisomic small chr.	7.00	4.15	versus	Monosomic small chr.	5.30	4.23	<0.0001	0.005
	Live birth	7.45	2.75	versus	Monosomic small chr.	5.30	4.23	<0.0001	<0.0001
					Monosomic medium chr.	5.40	3.00	<0.0001	0.001
					Monosomic large chr.	4.10	4.28	<0.0001	0.001
KIDScore	Trisomic small chr.	7.30	1.65	versus	Monosomic medium chr.	5.80	1.90	0.001	0.026
	Live birth	7.80	2.60	versus	Monosomic small chr.	6.30	1.65	0.001	0.019
					Monosomic medium chr.	5.80	1.90	<0.0001	0.001
					Monosomic large chr.	6.30	2.78	0.001	0.025

Each row tests the null hypothesis that the Group 1 and Group 2 distributions are the same.

p value*- nominal significance from a 2-sided Kruskal Wallis test.

[a] Nominal significance from a two-sided Kruskal-Wallis test.

[b] Adjusted for multiplicity using Bonferroni's correction.

Large chr, chromosomes 1-8 and X; medium chr: chromosomes 9-16; small chr, chromosomes 17-22 and Y; AI, artificial intelligence.

An extended list of multiple comparisons is available in Supplementary Table 5.

aneuploidies less than whole chromosome aneuploidies compared with euploid embryos (*Diakiw et al., 2022b*).

CONCLUSION

This study provides critical insights into the morphokinetic profiles of embryos with various chromosomal abnormalities, particularly focusing on how different types of aneuploidies impact embryo development. It was observed that monosomies delay embryo development significantly, resulting in slower progression through the key stages of blastulation. Complex aneuploidies also exhibited delayed development, but these were more challenging to distinguish using morphokinetic analysis alone. Trisomic embryos, especially those with medium and small chromosome trisomies, displayed developmental trajectories and time-lapse-based scoring similar to euploid embryos. Despite advances in AI-based selection tools, the present findings emphasize that current methodologies still struggle to differentiate accurately between embryos with subtle chromosomal variations, particularly trisomies. This underscores the need for further refinement of these tools to enhance their predictive accuracy, or to consider alternative non-invasive strategies to complement morphokinetic and time-lapse analysis, to ultimately improve clinical outcomes in assisted reproductive technology.

SUPPLEMENTARY MATERIALS

Supplementary material associated with this article can be found in the online version at doi:10.1016/j.rbmo.2025.104828.

REFERENCES

Ahlström, A., Berntsen, J., Johansen, M., Bergh, C., Cimadomo, D., Hardarson, T., Lundin, K., 2023. Correlations between a deep learning-based algorithm for embryo evaluation with cleavage-stage cell numbers and fragmentation. Reproductive Biomedicine Online 47, 103408.

Alfarawati, S., Fragouli, E., Colls, P., Stevens, J., Gutiérrez-Mateo, C., Schoolcraft, W.B., Katz-Jaffe, M.G., Wells, D., 2011. The relationship between blastocyst morphology, chromosomal abnormality, and embryo gender. Fertility and Sterility, 95 (2), 520–524.

Amir, H., Barbash-Hazan, S., Kalma, Y., Frumkin, T., Malcov, M., Samara, N., Hasson, J., Reches, A., Azem, F., Ben-Yosef, D., 2019. Time-lapse imaging reveals delayed development of embryos carrying unbalanced chromosomal translocations. Journal of Assisted Reproduction and Genetics 36 (2), 315–324.

Bamford, T., Easter, C., Montgomery, S., Smith, R., Dhillon-Smith, R.K., Barrie, A., Campbell, A., Coomarasamy, A., 2023. A comparison of 12 machine learning models developed to predict ploidy, using a morphokinetic meta-dataset of 8147 embryos. Human Reproduction 38 (4), 569–581.

Barrie, A., McDowell, G., Troup, S., 2021. An investigation into the effect of potential confounding patient and treatment parameters

on human embryo morphokinetics. Fertility and Sterility 115 (4), 1014–1022.
Basile, N., Nogales, M.delC., Bronet, F., Florensa, M., Riqueiros, M., Rodrigo, L., García-Velasco, J., Meseguer, M., 2014. Increasing the probability of selecting chromosomally normal embryos by time-lapse morphokinetics analysis. Fertility and Sterility 101, 699–704.
Berntsen, J., Rimestad, J., Lassen, J.T., Tran, D., Kragh, M.F., 2022. Robust and generalizable embryo selection based on artificial intelligence and time-lapse image sequences. PLoS One 17 (2), e0262661.
Campbell, A., Fishel, S., Bowman, N., Duffy, S., Sedler, M., Hickman, C.F., 2013a. Modelling a risk classification of aneuploidy in human embryos using non-invasive morphokinetics. Reproductive Biomedicine Online 26 (5), 477–485.
Campbell, A., Fishel, S., Bowman, N., Duffy, S., Sedler, M., Thornton, S., 2013b. Retrospective analysis of outcomes after IVF using an aneuploidy risk model derived from time-lapse imaging without PGS. Reproductive Biomedicine Online 27 (2), 140–146.
Capalbo, A., Rienzi, L., Cimadomo, D., Maggiulli, R., Elliott, T., Wright, G., Nagy, Z.P., Ubaldi, F.M., 2014. Correlation between standard blastocyst morphology, euploidy and implantation: an observational study in two centers involving 956 screened blastocysts. Human Reproduction 29 (6), 1173–1181.
Chavez, S.L., Loewke, K.E., Han, J., Moussavi, F., Colls, P., Munne, S., Behr, B., Reijo Pera, R.A., 2012. Dynamic blastomere behaviour reflects human embryo ploidy by the four-cell stage. Nature Communications 3, 1251.
Chawla, M., Fakih, M., Shunnar, A., Bayram, A., Hellani, A., Perumal, V., Divakaran, J., Budak, E., 2015. Morphokinetic analysis of cleavage stage embryos and its relationship to aneuploidy in a retrospective time-lapse imaging study. Journal of Assisted Reproduction and Genetics 32 (1), 69–75.
Ciray, H.N., Campbell, A., Agerholm, I.E., Aguilar, J., Chamayou, S., Esbert, M., Sayed, S., Time-Lapse User Group, 2014. Proposed guidelines on the nomenclature and annotation of dynamic human embryo monitoring by a time-lapse user group. Human Reproduction 29 (12), 2650–2660.
De Gheselle, S., De Sutter, P., Tilleman, K., 2020. In-vitro development of embryos derived from vitrified-warmed oocytes is delayed compared with embryos derived from fresh oocytes: a time-lapse sibling oocyte study. Reproductive Biomedicine Online 40 (1), 82–90.
De Martin, H., Bonetti, T.C.S., Nissel, C.A.Z., Gomes, A.P., Fujii, M.G., Monteleone, P.A.A., 2024. Association of early cleavage, morula compaction and blastocysts ploidy of IVF embryos cultured in a time-lapse system and biopsied for genetic test for aneuploidy. Scientific Reports 14 (1), 739.
De Munck, N., Bayram, A., Elkhatib, I., Liñán, A., Arnanz, A., Melado, L., Lawrenz, B., Fatemi, M.H., 2021. Segmental duplications and monosomies are linked to in vitro developmental arrest. Journal of Assisted Reproduction and Genetics 38 (8), 2183–2192.
Del Carmen Nogales, M., Bronet, F., Basile, N., Martínez, E.M., Liñán, A., Rodrigo, L., Meseguer, M., 2017. Type of chromosome abnormality affects embryo morphology dynamics. Fertility and Sterility 107 (1), 229–235. e2.
Diakiw, S.M., Hall, J.M.M., VerMilyea, M.D., Amin, J., Aizpurua, J., Giardini, L., Briones, Y.G., Lim, A.Y.X., Dakka, M.A., Nguyen, T.V., Perugini, D., Perugini, M., 2022a. Development of an artificial intelligence model for predicting the likelihood of human embryo euploidy based on blastocyst images from multiple imaging systems during IVF. Human Reproduction 37 (8), 1746–1759.
Diakiw, S.M., Hall, J.M.M., VerMilyea, M., Lim, A.Y.X., Quangkananurug, W., Chanchamroen, S., Bankowski, B., Stones, R., Storr, A., Miller, A., Adaniya, G., van Tol, R., Hanson, R., Aizpurua, J., Giardini, L., Johnston, A., Van Nguyen, T., Dakka, M.A., Perugini, D., Perugini, M., 2022b. An artificial intelligence model correlated with morphological and genetic features of blastocyst quality improves ranking of viable embryos. Reproductive Biomedicine Online 45 (6), 1105–1117.
Duval, A., Nogueira, D., Dissler, N., Maskani Filali, M., Delestro Matos, F., Chansel-Debordeaux, L., Ferrer-Buitrago, M., Ferrer, E., Antequera, V., Ruiz-Jorro, M., Papaxanthos, A., Ouchchane, H., Keppi, B., Prima, P.Y., Regnier-Vigouroux, G., Trebesses, L., Geoffroy-Siraudin, C., Zaragoza, S., Scalici, E., Sanguinet, P., Cassagnard, N., Ozanon, C., De La Fuente, A., Gómez, E., Gervoise Boyer, M., Boyer, P., Ricciarelli, E., Pollet-Villard, X., Boussommier-Calleja, A., 2023. A hybrid artificial intelligence model leverages multi-centric clinical data to improve fetal heart rate pregnancy prediction across time-lapse systems. Human Reproduction 38 (4), 596–608.
Fishel, S., Campbell, A., Montgomery, S., Smith, R., Nice, L., Duffy, S., Jenner, L., Berrisford, K., Kellam, L., Smith, R., D'Cruz, I., Beccles, A., 2017. Live births after embryo selection using morphokinetics versus conventional morphology: a retrospective analysis. Reproductive Biomedicine Online 35 (4), 407–416.
Gao, J., Yan, Z., Yan, L., Zhu, X., Jiang, H., Qiao, J., 2023. The effect of sperm DNA fragmentation on the incidence and origin of whole and segmental chromosomal aneuploidies in human embryos. Reproduction 166 (2), 117–124.
Gardner, D.K., Schoolcraft, W.B., 1999. Culture and transfer of human blastocysts. Curr. Opin. Obstet. Gynecol. 11 (6), 307–311.
Hori, K., Hori, K., Kosasa, T., Walker, B., Ohta, A., Ahn, H.J., Huang, T.T.F., 2023. Comparison of euploid blastocyst expansion with subgroups of single chromosome, multiple chromosome, and segmental aneuploids using an AI platform from donor egg embryos. Journal of Assisted Reproduction and Genetics 40 (6), 1407–1416.
Huang, T.T., Huang, D.H., Ahn, H.J., Arnett, C., Huang, C.T., 2019. Early blastocyst expansion in euploid and aneuploid human embryos: evidence for a non-invasive and quantitative marker for embryo selection. Reproductive Biomedicine Online 39 (1), 27–39.
Hur, C., Nanavaty, V., Yao, M., Desai, N., 2023. The presence of partial compaction patterns is associated with lower rates of blastocyst formation, sub-optimal morphokinetic parameters and poorer morphologic grade. Reproductive Biology and Endocrinology: 21 (1), 12.
Ivec, M., Kovacic, B., Vlaisavljevic, V., 2011. Prediction of human blastocyst development from morulas with delayed and/or incomplete compaction. Fertility and Sterility 96 (6), 1473–1478.e2.
Kahraman, S., Sahin, Y., Yelke, H., Kumtepe, Y., Tufekci, M.A., Yapan, C.C., Yesil, M., Cetinkaya, M., 2020. High rates of aneuploidy, mosaicism and abnormal morphokinetic development in cases with low sperm concentration. Journal of Assisted Reproduction and Genetics 37 (3), 629–640.
Kahraman, S., Yakin, K., Dönmez, E., Samli, H., Bahçe, M., Cengiz, G., Sertyel, S., Samli, M., Imirzalioğlu, N., 2000. Relationship between granular cytoplasm of oocytes and pregnancy outcome following intracytoplasmic sperm injection. Human Reproduction 15 (11), 2390–2393.
Kato, K., Ueno, S., Berntsen, J., Kragh, M.F., Okimura, T., Kuroda, T., 2023. Does embryo categorization by existing artificial intelligence, morphokinetic or morphological embryo selection models correlate with blastocyst euploidy rates? Reproductive Biomedicine Online 46 (2), 274–281.
Kirkegaard, K., Campbell, A., Agerholm, I., Bentin-Ley, U., Gabrielsen, A., Kirk, J., Sayed, S., Ingerslev, H.J., 2014. Limitations of a time-lapse blastocyst prediction model: a large multicentre outcome analysis. Reproductive Biomedicine Online 29 (2), 156–158.
Kirkegaard, K., Sundvall, L., Erlandsen, M., Hindkjær, J.J., Knudsen, U.B., Ingerslev, H.J., 2016. Timing of human preimplantation embryonic development is confounded by embryo origin. Human Reproduction 31 (2), 324–331.
Kramer, Y.G., Kofinas, J.D., Melzer, K., Noyes, N., McCaffrey, C., Buldo-Licciardi, J., McCulloh, D.H., Grifo, J.A., 2014. Assessing morphokinetic parameters via time lapse microscopy (TLM) to predict euploidy: are aneuploidy risk classification models universal? Journal of Assisted Reproduction and Genetics 31 (9), 1231–1242.
Kubicek, D., Hornak, M., Horak, J., Navratil, R., Tauwinklova, G., Rubes, J., Vesela, K., 2019. Incidence and origin of meiotic whole and segmental chromosomal aneuploidies detected by karyomapping. Reproductive Biomedicine Online 38 (3), 330–339.
Lee, C.I., Chen, C.H., Huang, C.C., Cheng, E.H., Chen, H.H., Ho, S.T., Lin, P.Y., Lee, M.S., Lee, T.H., 2019. Embryo morphokinetics is potentially associated with clinical outcomes of single-embryo transfers in preimplantation genetic testing for aneuploidy cycles. Reproductive Biomedicine Online 39 (4), 569–579.
Liu, Y., Chapple, V., Feenan, K., Roberts, P., Matson, P., 2015. Time-lapse videography of human embryos: Using pronuclear fading rather than insemination in IVF and ICSI cycles removes inconsistencies in time to reach early cleavage milestones. Reproductive Biology 15 (2), 122–125.
Martín, Á., Rodrigo, L., Beltrán, D., Meseguer, M., Rubio, C., Mercader, A., de Los Santos, M.J, 2021. The morphokinetic signature of mosaic embryos: evidence in support of their own

genetic identity. Fertility and Sterility 116 (1), 165–173.
Minasi, M.G., Colasante, A., Riccio, T., Ruberti, A., Casciani, V., Scarselli, F., Spinella, F., Fiorentino, F., Varricchio, M.T., Greco, E., 2016. Correlation between aneuploidy, standard morphology evaluation and morphokinetic development in 1730 biopsied blastocysts: a consecutive case series study. Human Reproduction 31 (10), 2245–2254.
Montgomery, K., Montgomery, S., Campbell, A., Nash, D.M., 2023. A comparison of the morphokinetic profiles of embryos developed from vitrified versus fresh oocytes. Reproductive Biomedicine Online 47 (1), 51–60.
Mumusoglu, S., Ozbek, I.Y., Sokmensuer, L.K., Polat, M., Bozdag, G., Papanikolaou, E., Yarali, H., 2017a. Duration of blastulation may be associated with ongoing pregnancy rate in single euploid blastocyst transfer cycles. Reproductive Biomedicine Online 35, 633–639.
Mumusoglu, S., Yarali, I., Bozdag, G., Ozdemir, P., Polat, M., Sokmensuer, L.K., Yarali, H., 2017. Time-lapse morphokinetic assessment has low to moderate ability to predict euploidy when patient- and ovarian stimulation-related factors are taken into account with the use of clustered data analysis. Fertility and Sterility 107 (2), 413–421.e4.
Munné, S., 2006. Chromosome abnormalities and their relationship to morphology and development of human embryos. Reproductive Biomedicine Online 12 (2), 234–253.
Muñoz, M., Cruz, M., Humaidan, P., Garrido, N., Pérez-Cano, I., Meseguer, M., 2013. The type of GnRH analogue used during controlled ovarian stimulation influences early embryo developmental kinetics: a time-lapse study. European Journal of Obstetrics, Gynecology, and Reproductive Biology 168 (2), 167–172.
Navarro, P.A., de Araújo, M.M., de Araújo, C.M., Rocha, M., dos Reis, R., Martins, W., 2009. Relationship between first polar body morphology before intracytoplasmic sperm injection and fertilization rate, cleavage rate, and embryo quality. International Journal of Gynaecology and Obstetrics 104 (3), 226–229.
Navratil, R., Horak, J., Hornak, M., Kubicek, D., Balcova, M., Tauwinklova, G., Travnik, P., Vesela, K., 2020. Concordance of various chromosomal errors among different parts of the embryo and the value of re-biopsy in embryos with segmental aneuploidies. Molecular Human Reproduction 26 (4), 269–276.
Patel, D.V., Shah, P.B., Kotdawala, A.P., Herrero, J., Rubio, I., Banker, M.R., 2016. Morphokinetic behavior of euploid and aneuploid embryos analyzed by time-lapse in embryoscope. Journal of Human Reproductive Sciences 9 (2), 112–118.
Pirtea, P., De Ziegler, D., Tao, X., Sun, L., Zhan, Y., Ayoubi, J.M., Seli, E., Franasiak, J.M., Scott, Jr, R.T., 2021. Rate of true recurrent implantation failure is low: results of three successive frozen euploid single embryo transfers. Fertility and Sterility 115 (1), 45–53.
Pribenszky, C., Nilselid, A.M., Montag, M., 2017. Time-lapse culture with morphokinetic embryo selection improves pregnancy and live birth chances and reduces early pregnancy loss: a meta-analysis. Reproductive Biomedicine Online 35 (5), 511–520.
Pylyp, L.Y., Spynenko, L.O., Verhoglyad, N.V., Mishenko, A.O., Mykytenko, D.O., Zukin, V.D., 2018. Chromosomal abnormalities in products of conception of first-trimester miscarriages detected by conventional cytogenetic analysis: a review of 1000 cases. Journal of Assisted Reproduction and Genetics 35 (2), 265–271.
Qi, S.T., Liang, L.F., Xian, Y.X., Liu, J.Q., Wang, W., 2014. Arrested human embryos are more likely to have abnormal chromosomes than developing embryos from women of advanced maternal age. Journal of Ovarian Research 7, 65.
Quinn, M.M., Marsh, P., Ribeiro, S., Simbulan, R.K., Rosen, M.P., 2022. A deep dive into the morphokinetics and ploidy of low-quality blastocysts. F&S Reports 3 (3), 231–236.
Rajendran, S., Brendel, M., Barnes, J., Zhan, Q., Malmsten, J.E., Zisimopoulos, P., Sigaras, A., Ofori-Atta, K., Meseguer, M., Miller, K.A., Hoffman, D., Rosenwaks, Z., Elemento, O., Zaninovic, N., Hajirasouliha, I., 2023. Automatic ploidy prediction and quality assessment of human blastocyst using time-lapse imaging. bioRxiv 2023.08.31.555741.
Rienzi, L., Ubaldi, F., Iacobelli, M., Minasi, M.G., Romano, S., Greco, E., 2005. Meiotic spindle visualization in living human oocytes. Reproductive Biomedicine Online 10 (2), 192–198.
Schachter-Safrai, N., Karavani, G., Esh-Broder, E., Levitas, E., Wainstock, T., Har-Vardi, I., Ben-Meir, A., 2021. High ovarian response to ovarian stimulation: effect on morphokinetic milestones and cycle outcomes. Journal of Assisted Reproduction and Genetics 38 (12), 3083–3090.
Setti, A., Braga, D., Guilherme, P., Iaconelli, Jr, A., Borges, Jr, E., 2022. High oocyte immaturity rates affect embryo morphokinetics: lessons of time-lapse imaging system. Reproductive Biomedicine Online 45 (4), 652–660.
Shenoy, C.C., Khan, Z., Coddington, C.C., Stewart, E.A., Morbeck, D.E., 2021. Symmetry at the 4-cell stage is associated with embryo aneuploidy. Reproductive Sciences 28 (12), 3473–3479.
Simopoulou, M., Sfakianoudis, K., Maziotis, E., Tsioulou, P., Grigoriadis, S., Rapani, A., Giannelou, P., Asimakopoulou, M., Kokkali, G., Pantou, A., Nikolettos, K., Vlahos, N., Pantos, K., 2021. PGT-A: who and when? A systematic review and network meta-analysis of RCTs. Journal of Assisted Reproduction and Genetics 38 (8), 1939–1957.
Spinella, F., Bronet, F., Carvalho, F., Coonen, E., De Rycke, M., Rubio, C., Goossens, V., Van Montfoort, A., 2023. ESHRE PGT Consortium data collection XXI: PGT analyses in 2018. Human Reproduction Open 2023 (2), hoad010.
Tartia, A.P., Wu, C.Q., Gale, J., Shmorgun, D., Léveillé, M.C., 2022. Time-lapse KIDScoreD5 for prediction of embryo pregnancy potential in fresh and vitrified-warmed single-embryo transfers. Reproductive Biomedicine Online 45 (1), 46–53.
Tran, D., Cooke, S., Illingworth, P.J., Gardner, D.K., 2019. Deep learning as a predictive tool for fetal heart pregnancy following time-lapse incubation and blastocyst transfer. Human Reproduction 34 (6), 1011–1018.
Tschare, L., Ennemoser, A., Carli, L., Vaccari, E., Feichtinger, M., 2023. Impact of maternally derived meiotic aneuploidies on early embryonic development in vitro. Journal of Assisted Reproduction and Genetics 40 (11), 2715–2723.
Viotti, M., Victor, A.R., Barnes, F.L., Zouves, C.G., Besser, A.G., Grifo, J.A., Cheng, E.H., Lee, M.S., Horcajadas, J.A., Corti, L., Fiorentino, F., Spinella, F., Minasi, M.G., Greco, E., Munné, S., 2021. Using outcome data from one thousand mosaic embryo transfers to formulate an embryo ranking system for clinical use. Fertility and Sterility 115 (5), 1212–1224.
Zore, T., Kroener, L.L., Wang, C., Liu, L., Buyalos, R., Hubert, G., Shamonki, M., 2019. Transfer of embryos with segmental mosaicism is associated with a significant reduction in live-birth rate. Fertility and Sterility 111 (1), 69–76.
Zou, Y., Pan, Y., Ge, N., Xu, Y., Gu, R., Li, Z., Fu, J., Gao, J., Sun, X., Sun, Y., 2022. Can the combination of time-lapse parameters and clinical features predict embryonic ploidy status or implantation? Reproductive Biomedicine Online 45 (4), 643–651.
Zou, Y., Sui, Y., Fu, J., Ge, N., Sun, X., Sun, Y., 2024. The morphokinetic signature of human blastocysts with mosaicism and the clinical outcomes following transfer of embryos with low-level mosaicism. Journal of Ovarian Research 17 (1), 10.

Received 11 September 2024; received in revised form 30 November 2024; accepted 10 January 2025.